CRYSTAL GROWTH & DESIGN Article
2009, Vol. 9
5184–5189

DOI: 10.1021/cg900580r

Structural Characteristics and Annealing Effect of ZnO Epitaxial Films Grown by Atomic Layer Deposition

S. Yang,[#] B. H. Lin,[#,†] W.-R. Liu,[#,†] J.-H. Lin,[#] C.-S. Chang,[#] C.-H. Hsu,*[,†,#] and W. F. Hsieh*[,#,‡]

[#]*Department of Photonics & Institute of Electro-Optical Engineering National Chiao Tung University, Hsinchu 30050, Taiwan,* [†]*Division of Scientific Research, National Synchrotron Radiation Research Center, Hsinchu 30076, Taiwan, and* [‡]*Institute of Electro-Optical Science & Engineering, National Cheng Kung University, Tainan 70101, Taiwan*

Received May 29, 2009; Revised Manuscript Received September 20, 2009

ABSTRACT: Structural characteristics of the ZnO epitaxial films grown on *c*-plane sapphire by the atomic layer deposition method were thoroughly studied. The in-plane axes of the *c*-plane oriented ZnO layers are predominantly aligned with that of the sapphire substrate, yielding the relationship of $\{10\bar{1}0\}_{ZnO} \parallel \{10\bar{1}0\}_{Al_2O_3}$. The minor orientation with a 30° in-plane twist configuration, that is, $\{10\bar{1}0\}_{ZnO} \parallel \{11\bar{2}0\}_{Al_2O_3}$, which is more commonly observed in ZnO films grown by metal organic chemical vapor deposition, pulsed laser deposition, and other methods, only amounts to less than 3% and can be eliminated by thermal annealing. The structure of the ZnO epi-films exhibits significantly improvement upon thermal annealing, and intrinsic types of basal plane stacking faults are the predominant structural defects in the ZnO after thermal treatment. The effect of post growth thermal treatment is reported in this work.

Introduction

ZnO with hexagonal wurtzite structure (lattice constants $a = 3.2438$ and $c = 5.2036$ Å) has many attractive properties such as a large direct wide band gap ($E_g = 3.3$ eV) and large exciton binding energy (~60 meV) at room temperature, native tendency of *n*-type electric property, piezoelectricity, and transparency. These properties make ZnO thin film a potential material for many applications such as the ultraviolet light emitters,[1,2] piezoelectric transducers,[3] transparent electronics,[4−6] surface acoustic wave devices,[7] and solar cells.[8,9] The *c*-plane sapphire (α-Al_2O_3 with a rhombohedral crystal structure and lattice constants $a = 4.759$ Å and $c = 12.992$ Å) is commonly adopted as the substrate for ZnO growth because reasonable costs and good quality of the ZnO obtained. On *c*-sapphire, ZnO preferentially grows with its *c*-axis aligned with the *c*-axis of substrate.

Molecular beam epitaxy (MBE), metal organic chemical vapor deposition (MOCVD),[6,10] and pulsed laser deposition (PLD)[11−13] have been widely employed to grow ZnO epitaxial films with high structural quality. Recently, atomic layer deposition (ALD) has attracted much attention for its application in ZnO growth.[14−21] ALD is a technique based on the sequential use of self-terminating gas−solid reactions that bear many practical advantages such as large-area deposition, high uniformity, high reproducibility, high covering ratio, low growth temperature, and the ability of producing sharp and tailored interfaces.[22] Moreover, the merit of accurate thickness control renders ALD particularly suitable for the fabrication of high quality multiquantum-well (MQW) structures.

In this paper, the ALD method is employed to fabricate ZnO epi-films on *c*-plane sapphire. The structural characteristics of the as-grown and thermally annealed ZnO films were thoroughly studied by both scattering and microscopic methods, including X-ray diffraction (XRD), transmission electron microscopy (TEM), and atomic force microscopy (AFM). The effects of thermal annealing on the structural properties are investigated.

Experimental Procedures

The *c*-plane (0001) oriented sapphire was cleaned by sequential D.I. water/acetone/D.I. water rinse for 5 min/5 min/5 min and then blown dry with N_2 gas. The cleaned sapphire substrate was then loaded into the ALD reactor (SYSKEY Ltd., Taiwan), heated to 200 °C, and held at this temperature for 30 min. Diethylzinc (DEZn with chemical formula of $Zn(C_2H_5)_2$ and purity 4N8) and H_2O (D. I. water of resistivity 18 MΩ·cm), kept in reservoirs at 25 °C, were used as zinc and oxygen precursors, respectively. The growth cycle consists of precursor exposures and N_2 purge following the sequence of DEZn/N_2/H_2O/N_2 with corresponding duration of 5 s/15 s/5 s/15 s. After each N_2 purging, the reactor was pumped down to $\sim 1 \times 10^{-2}$ Torr. Precursor introduction was done by opening the inlet valve between the reservoir and reactor chamber while the outlet valve was closed; no carrier gas was employed. The pressures of the DEZn and H_2O in the reactor chamber were approximately 7 and 17 Torr, respectively, monitored by a vacuum gauge. The substrate temperature was maintained at 200 °C under a vacuum of 1−2 Torr during the deposition. The reaction was repeated 200 times for all the studied samples. Ideally, two cycles of reaction yield a unit cell of ZnO along the *c*-axis; 200 cycles would lead to 100 unit cells along the growth direction equivalent to a thickness of about 52 nm. Thermal annealing was performed at temperatures varying from 300 to 800 °C for 1.5 h in pure oxygen gas at 1 atm.

The X-ray measurements were conducted using a four-circle diffractometer at beamline BL13A of National Synchrotron Radiation Research Center (NSRRC) with an incident wavelength 1.02473 Å. Two pairs of slits located between the sample and a NaI scintillation detector were employed and yielded a typical resolution of better than 1×10^{-3} Å^{-1}. Surface morphology and roughness of the ZnO layer were measured by AFM (Veeco Dimension 5000 Scanning Probe Microscope, D5000). Cross sectional TEM specimens with the thickness of about 90 ± 10 nm were prepared by focused ion beam (FIB). TEM images were taken with a Philips TECNAI-20 field emission gun type TEM.

*Authors to whom correspondence should be addressed. E-mail: chsu@nsrrc.org.tw (C.-H.H.); wfhsieh@mail.nctu.edu.tw (W.F.H.).

 © 2009 American Chemical Society

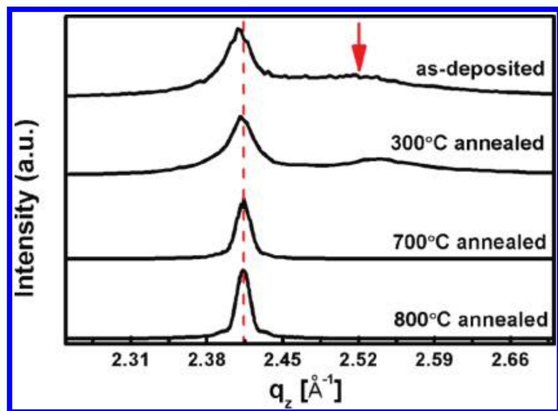

Figure 1. The radial scans ($\theta-2\theta$ scan) along the surface normal of the as-deposited ZnO and those annealed at 300, 700, and 800 °C. The red broken line marks the position of bulk ZnO (0002) reflection. The arrow indicates the location corresponding to the interplanar spacing of ZnO ($10\bar{1}1$).

Results and Discussion

Figure 1 illustrates the radial scan ($\theta-2\theta$ scan) along the surface normal of an as-deposited ZnO layer and the samples annealed at 300, 700, and 800 °C. The pronounced peak centered at q_z, momentum transfer along the surface normal, $\sim$2.409 Å^{-1} observed in the as-deposited sample yields an interplanar spacing $\sim$ 2.608 Å. This value is 0.24% larger than the d-spacing of bulk ZnO (0002) planes, d_{0002}; we assigned this peak to ZnO (0002) reflection. At the higher q_z side, a broad shoulder centered at $\sim$2.53 Å^{-1} is attributed to the ZnO ($10\bar{1}1$) reflection. Besides the reflections from sapphire substrate, no other peak originated from ZnO was observed, indicating the as-deposited ZnO layer is predominantly c-plane oriented with a coexisting minor ($10\bar{1}1$) orientation. It is worth mentioning that the ($10\bar{1}0$) plane was reported to be the preferential surface orientation in many ALD grown ZnO films, especially those grown on substrates such as Si (001)[15,16] and fused glass[23] or deposited at low temperatures.[19] No trace of the ($10\bar{1}0$) oriented grains was detected in our samples. This is attributed to the hexagonal symmetry of the c-sapphire, which strongly favors the growth of c-plane ZnO with compatible symmetry.[17,18] The other factor in favor of the growth of high quality c-plane ZnO is the long purging time used in our case. The simultaneous enhancement of (0001) growth and improvement of crystalline quality with prolonged purging time was reported by Wójcik et al.[19] Longer purging time provides not only more complete removal of physically adsorbed surface species and volatile byproduct but also a longer time for element diffusion to prepare a better surface for subsequent reaction.

Upon thermal annealing, the ZnO ($10\bar{1}1$) reflection disappears accompanied by the sharpening up and intensity enhancement of the ZnO (0002) reflection, a sign of increasing structural coherence along the growth direction. Moreover, the lattice parameter along the c-axis systematically decreases with increasing annealing temperature as revealed by the shift of the (0002) reflection to the higher q_z side and approaches the bulk value, as marked by the dashed line, to within 0.02% after 800 °C annealing.

The ZnO (0002) θ-rocking curves of the as-deposited and annealed samples, with the intensity normalized to corresponding peak intensity, are illustrated in Figure 2a. All the curves are composed of a shape peak (P_S) with typical full

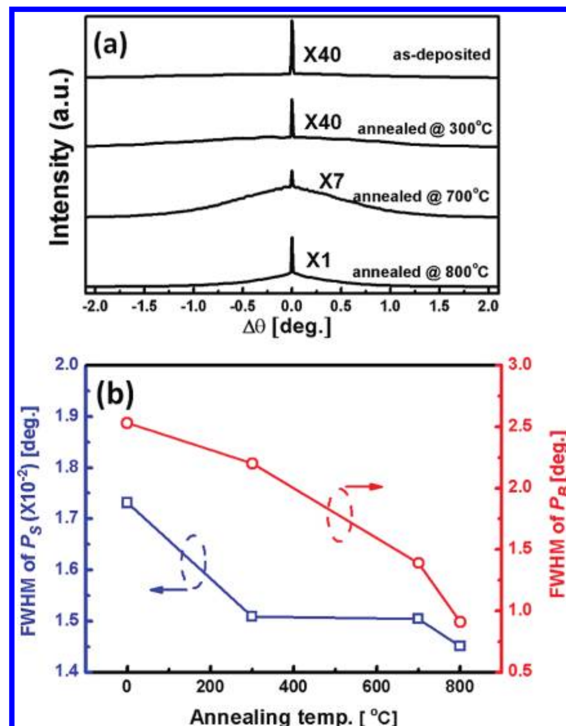

Figure 2. (a) The θ-rocking curves of the as-deposited and annealed ZnO layers. Each curve is a superposition of a sharp (P_S) and a broad peak (P_B). (b) The variation of the fwhm of P_S and P_B as a function of annealing temperature.

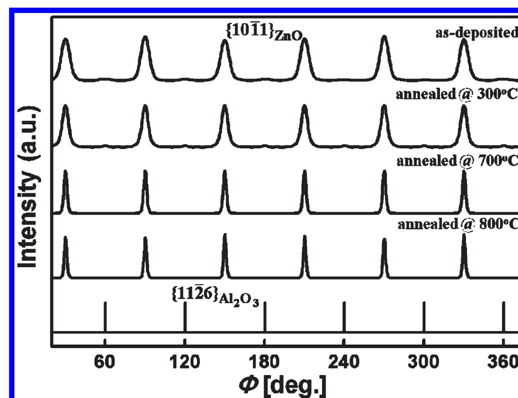

Figure 3. The ϕ-scan across the off-normal ZnO {$10\bar{1}1$} reflection of as-deposited and annealed ZnO layers, together with the ϕ-scan across sapphire {$11\bar{2}6$} shown at the bottom.

width at half-maximum (fwhm) of less than 0.02° superimposed with a broad peak (P_B) whose line width is 2 orders of magnitude larger than the central sharp peak. The broad component is attributed to the diffuse scattering from the structural defects, such as dislocations, and misoriented grains. Such a pronounced diffuse component has hardly been observed in ZnO epi-layers grown by PLD or MOCVD and indicates the intrinsic difference between the structural characteristics of the ZnO layers grown by ALD and other methods. Upon annealing the fwhm of the sharp component showed mild improvement from 0.017° to 0.015°, as shown in Figure 2b, and these values are comparable to the fwhm of sapphire (0006) reflection, 0.013°. In contrast, the fwhm of broad component exhibits a monotonic reduction from 2.53° for the as-deposited film to 0.91° for the 800 °C annealed sample and their integrated intensity also drastically decreases

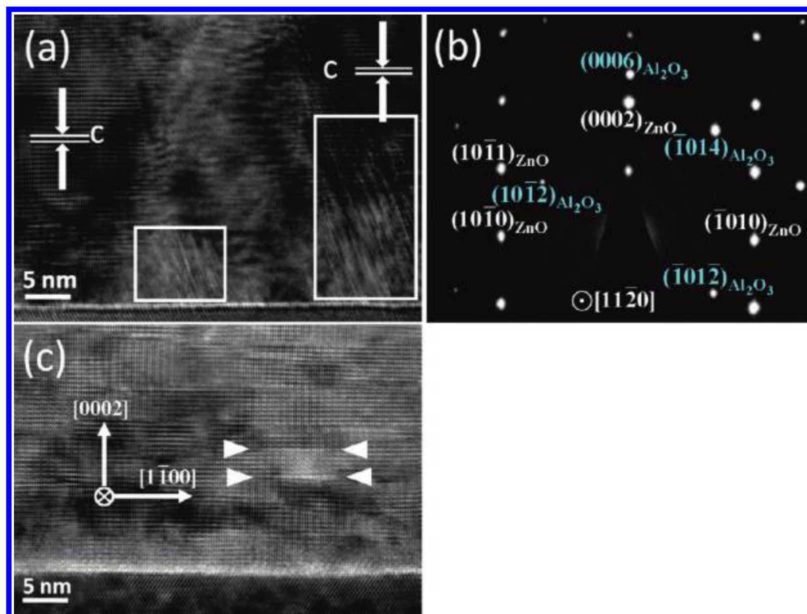

Figure 4. (a) The cross sectional TEM image of the as-deposited ZnO epi-layer along the $[11\bar{2}0]$ zone axis, (b) the SAED pattern, and (c) the image of 800 °C annealed sample taken under the same pole.

with elevated annealing temperature, evidencing the significant improvement of structural perfection by the thermal treatment.

In order to determine the epitaxial relationship between the ZnO layers and the substrates, we performed azimuthal cone scans (ϕ-scans) across the off-normal ZnO$\{10\bar{1}1\}$ and sapphire $\{11\bar{2}6\}$ reflections, as illustrated in Figure 3. For both as-deposited and annealed ZnO layers, the scans across the ZnO $\{10\bar{1}1\}$ reflections show 6-fold symmetry confirming the hexagonal symmetry. The angular positions of these peaks are offset from that of the six sapphire $\{11\bar{2}6\}$ reflections by 30° and yield the in-plane relationship of $\{10\bar{1}0\}_{ZnO} \parallel \{10\bar{1}0\}_{Al_2O_3}$, the "aligned orientation". It is also noticed that the fwhm of the ZnO $\{10\bar{1}1\}$ peaks drastically decreases from 6.75° for the as-deposited sample to 2.48° for the sample after 800 °C thermal treatment, again indicating the significant improvement in twist deformation upon annealing. Carefully examining the ϕ-scan of the as-deposited sample, we found another set of weak peaks with 6-fold symmetry appearing at the same angular position as sapphire $\{11\bar{2}6\}$. This observation reveals the existence of a small fraction of *c*-plane ZnO has $\{10\bar{1}0\}_{ZnO} \parallel \{11\bar{2}0\}_{Al_2O_3}$ orientation, the "twisted orientation". Determined from the integrated intensity, the fraction of the minor twisted orientation decreases with annealing temperature from ~4.2% for as-deposited film to less than 0.03% after 800 °C thermal annealing.

The twisted orientation, in which the lattice of ZnO is aligned with the oxygen sublattice in sapphire, is most commonly observed for ZnO epi-films grown on *c*-sapphire.[11,24−26] Its lattice mismatch with sapphire, 18.3%, is smaller than the 31.8% of the aligned orientation, in which the ZnO lattice is aligned with the Al sublattice in sapphire. Intuitively, the twisted orientation is energetically favorable, and indeed most of the ZnO epi-layers grown on *c*-plane sapphire by PLD and MOCVD, VPE have this orientation.[10,25,26] The aligned in-plane orientation has been reported on ZnO epi-films grown by PLD and magnetron sputtering at low deposition temperatures ($T < 600$ °C).[27−30] In those works, the fraction of the domains with the aligned orientation increases with decreasing growth temperature and/or lower deposition rate.

The orientation of the epi-films is a result of the competition between the interfacial bonding, elastic energy, and surface energy. In view of the energy of interfacial bonding, the much larger bond energy of Al−O (511 kJ/mol) bond than the Zn−O bond (271 kJ/mol) favors the O−Al−O−Zn configuration, that is, the O in ZnO bonds with the Al in sapphire substrate, and leads to the alignment of Zn terminated ZnO lattice with Al sublattice.[27] However, from the aspect of smaller lattice mismatch and higher thermodynamic stability of O-terminated ZnO surface,[31] the configuration with twisted orientation is preferred. Ohkubo et al. attributed the prevalence of the aligned orientation at low temperatures to Al termination of sapphire surface and the dominance of local interface energy when the growth process is kinetics limited.[24,26] According to this argument, the low operation temperature of ALD favors the formation of observed aligned orientation, but the interfacial bonding mechanism should be different because of the alternative formation of Zn and O atomic layers during two separate half reactions.

The topmost surface of a sapphire wafer after wet-cleaning is terminated by hydroxyl groups due to its high stability. It is a known difficulty of creating an OH free sapphire surface not mentioning the surface prepared by wet-cleaning and mild heating pretreatment adopted in our process.[32] According to the ALD growth sequence, the zinc precursor DEZn with the chemical structure of $CH_3{-}CH_2{-}Zn{-}CH_2{-}CH_3$ is first supplied onto the substrate surface. One ethyl of the DEZn reacts with the hydroxyl at the sapphire surface and leaves the zinc atom bonded with the oxygen at the substrate surface. Volatile organic byproduct ethane is pumped away and the residual functional group ethyl prevents the continuous growth of deposited material due to the self-limiting effect. Subsequently introduced H_2O reacted with the ethyl group and formed a -Zn−O−H terminated surface.[25] After this point, the rest of the film growth can be considered as homoepitaxy. The initial bonding of DEZn to sapphire, $-Al{-}O{-}Zn{-}CH_2{-}CH_3$, anchors the orientation of the ZnO layer, which follows the atomic arrangement of the Al sublattice in sapphire and yields the observed aligned orientation, that is, $\{10\bar{1}0\}_{ZnO} \parallel \{10\bar{1}0\}_{Al_2O_3}$.

It is well-known that structural properties obtained by XRD are an ensemble average over the macroscopic illuminated volume, typical of mm^3. On the contrary, microscopy probes microscopic features over a much more localized region. As a complement, we also performed TEM measurements on the ZnO epi-layers. Illustrated in Figure 4a is a cross sectional TEM image taken along the $[11\bar{2}0]_{Al_2O_3}$ zone axis, in which ZnO grains with planes of 5.2 Å interplanar spacing parallel to the interface can be well resolved. The selected area electron diffraction (SAED) pattern (Figure 4b) confirmed the $(0001) < 1\bar{1}00 >_{ZnO} \parallel (0001) < 1\bar{1}00 >_{Al_2O_3}$ orientation in agreement with XRD observation. However, numerous misoriented grains, as enclosed by the rectangles in Figure 4a and defects of various kinds distribute throughout the grown film. Figure 4c is the micrograph of the 800 °C annealed sample taken under the same pole, which exhibits drastic structural improvement. Moreover, many contrast lines lying in the basal planes with lateral extension of the order of 10 nm (some of them are marked by arrows) were observed. These lines were verified to be basal plane stacking faults as described below and represented the majority of structural defects found in annealed ALD grown c-ZnO epi-films.

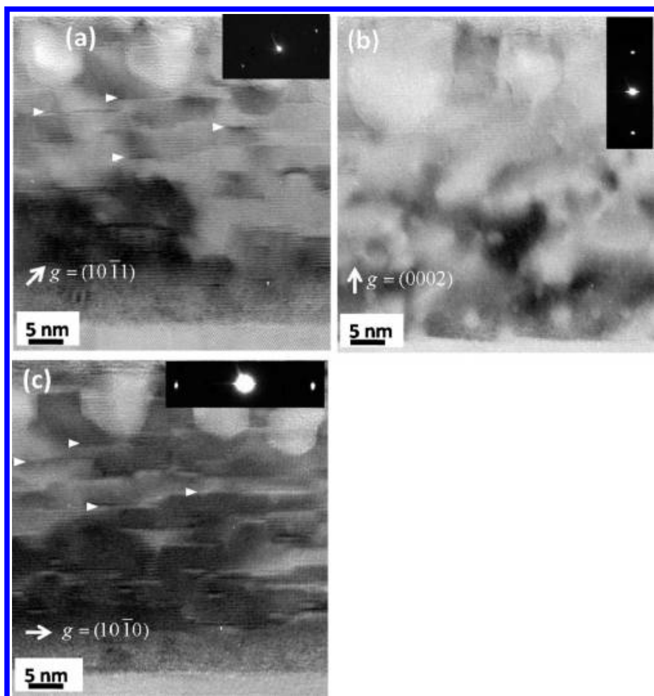

Figure 5. The bright-filed images of the ZnO layer annealed at 800 °C with diffraction vector $\boldsymbol{g}$ set to (a) $(10\bar{1}1)$, (b) (0002), and (c) $(10\bar{1}0)$. The insets show the corresponding diffraction peaks used under two-beam condition.

To characterize the nature of the lateral lines, we performed diffraction contrast analysis on the images of the 800 °C annealed sample. The bright field images of the same region taken along the $[11\bar{2}0]$ pole and with diffraction vector $\boldsymbol{g}$ set to $(10\bar{1}1)$, (0002), and $(10\bar{1}0)$ are shown in Figure 5, panels a, b, and c, respectively. Depending on the type of error in stacking sequence or equivalently the displacement vector $\boldsymbol{R}$, which defines the relative displacement between the unfaulted lattices above and below the fault, the basal plane stacking faults in wurtzite crystal structure are generally divided into three types: two intrinsic ones named I_1 and I_2 and an extrinsic one named E. The displacement vectors associated with the I_1, I_2, and E type of basal plane stacking faults are $^1/_6\langle 2\bar{2}03\rangle$, $^1/_3\langle 1\bar{1}00\rangle$, and $^1/_2\langle 0001\rangle$, respectively.[33−35] According to the extinction rules for stacking faults in the TEM image, a stacking fault will be out of contrast if the dot product of its displacement vector $\boldsymbol{R}$ with the diffraction vector $\boldsymbol{g}$ used for imaging equals $2\pi n$, where $n = 0, \pm1, \pm2, ...$[34,35] Consequently, all three types of stacking faults are visible in image with $\boldsymbol{g} = (10\bar{1}1)$ and out of contrast as $\boldsymbol{g} = (0002)$. In the case of $\boldsymbol{g} = (10\bar{1}0)$, only intrinsic stacking faults of types I_1 and I_2 are in contrast. Examining the images taken under different diffraction vectors, we found about all the lateral lines visible in Figure 5a with $\boldsymbol{g} = (10\bar{1}1)$ became out of contrast in Figure 5b with $\boldsymbol{g} = (0002)$, confirming that basal plane

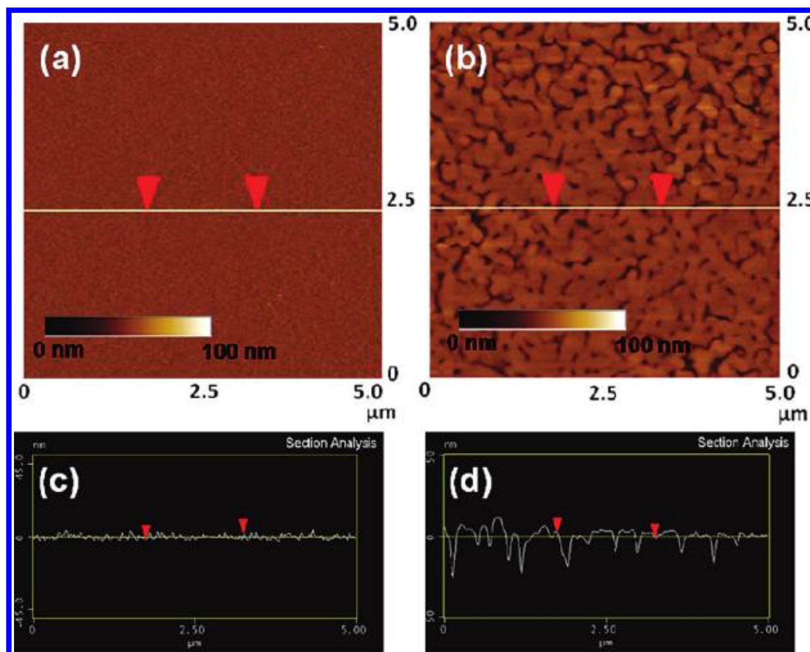

Figure 6. The AFM images of the (a) as-deposited and (b) annealed ZnO layers. The scan image profiles of the as-deposited and annealed samples are shown in (c) and (d), respectively.

stacking faults are indeed the major structural defects in the 800 °C annealed sample. Furthermore, the absence of an obvious difference in the spatial distribution of the lines found in images taken under $g = (10\bar{1}1)$ and $(10\bar{1}0)$, shown respectively in Figure 5b,c, reveals that the stacking faults belong to the intrinsic type. Unfortunately, we cannot further verify the type of stacking faults, I_1 or I_2. These lines are due to limited accessible diffraction vector under experimental geometry.

Unlike the ZnO epi-layers grown by PLD[12] and p-MBE[26] on *c*-sapphire where edge-type threading dislocations are the dominant structural defects in the film bulk, basal plane stacking faults are the majority of structural defects found in ALD grown c-ZnO epi-films. This also explains the small line width in the θ-rocking curve of ZnO (0002) reflection, which is not sensitive to the basal plane stacking faults. The diversity in characteristic structural features is related to the fundamental difference in the growth mechanism of those methods. In the case of PLD deposition, a plume of materials liberated from the target, consisting of a variety of energetic species, such as atoms, ions, and small clusters of the ZnO are deposited on the surface and the growth of ZnO film on *c*-sapphire proceeded via island nucleation followed by lateral extension.[36] Such a growth mode results in a film of a columnar structure surrounded by grain boundaries with a high density of threading dislocations.[12] In contrast, the intrinsic layer-by-layer growth nature of the ALD method unfavors the initial island nucleation and suppresses the formation of threading dislocations. Apparently, 800 °C annealing results in the grain growth and stimulates the precipitation of point defects such as vacancies or interstitials and/or the dissociation of dislocations together with the slip of partial dislocations, which are known as the most likely mechanisms for the generation of basal plane stacking faults.[34]

In additional to the crystalline structure, we also studied the effect on the surface morphology by thermal treatment. Voids were found in some areas near the film/air interface in the cross section TEM micrographs of the annealed sample (not shown). This explains the increase of surface roughness and the decrease of mass density near the film surface region in the annealed samples as revealed by X-ray reflectivity measurements. Figure 6a,b shows, respectively, the surface morphology before and after 800 °C annealing measured by AFM; Figure 6, panels c and d, are the corresponding section profiles of the scans along the surface. Grain growth and the development of voids between the grains are induced by thermal treatment and lead to the increase of root-mean-square roughness from 1.64 to 5.75 nm. The similar variation of surface morphology and the increase of grain size resulting from the post annealing have also been reported by other groups and are attributed to the recrystallization of the ZnO grains.[16-18]

Conclusion

The structural characteristics of the ALD grown ZnO epitaixal films on *c*-plane sapphire together with the influence of thermal annealing were thoroughly studied. The ZnO films are *c*-plane oriented. The *d*-spacing along the growth direction of the as-deposited ZnO layer is 0.24% larger than the bulk value and progressively decreases and approaches the bulk value with increasing annealing temperature. The in-plane epitaxial relationship of $\{10\bar{1}0\}_{ZnO} \parallel \{10\bar{1}0\}_{Al_2O_3}$ is confirmed from the ϕ-scan data of ZnO $\{10\bar{1}1\}$ and sapphire $\{11\bar{2}6\}$ reflections. This orientation is the same as that of ZnO grown on *c*-plane sapphire at low temperatures by the PLD method.[27] After annealing at high temperatures, the crystalline quality exhibits drastic improvement. The diffraction contrast analysis of the cross-section TEM images reveals that intrinsic basal plane stacking faults are the dominant structural defects of the annealed ZnO layers, different from the PLD grown ZnO layers where threading dislocations are the predominant defects. The diversity in the dominant type of structural defects was attributed to the fundamental difference in the growth mechanisms of the two methods.

Acknowledgment. The authors would like to thank Dr. H. S. Sheu of NSRRC for his constructive comments and valuable discussions. This work is partly supported by National Science Council of Taiwan under Grants NSC-96-2628-M-009-001-MY3 and NSC 96-2113-M-007-025-MY2.

Supporting Information Available: Flow chart illustrating the sequence and duration of each step within a deposition cycle. This material is available free of charge via the Internet at http://pubs.acs.org.

References

(1) Tsukazaki, A.; Ohtomo, A.; Onuma, T.; Ohtani, M.; Makino, T.; Sumiya, M.; Ohtani, K.; Chichibu, S. F.; Fuke, S.; Segawa, Y.; Ohno, H.; Koinuma, H.; Kawasaki, M. *Nat. Mater.* **2005**, *4*, 42.
(2) Lim, J. H.; Kang, C. K.; Kim, K. K.; Park, I. K.; Hwang, D. K.; Park, S. J. *Adv. Mater.* **2006**, *18*, 2720.
(3) Smith, A. *Thin Solid Films* **2000**, *376*, 47–55.
(4) Hao, X. T.; Tan, L. W.; Ong, K. S.; Zhu, F. R. *J. Cryst. Growth* **2006**, *287*, 44.
(5) Shukla, R. K.; Srivastava, A.; Srivastava, A.; Dubey, K. C. *J. Cryst. Growth* **2006**, *294*, 427.
(6) Jo, J.; Seo, O.; Choi, H.; Lee, B. *Appl. Phys. Express* **2008**, *1*, 041202.
(7) Tang, I. T.; Wang, Y. C.; Hwang, W. C.; Hwang, C. C.; Wu, N. C.; Houng, M. P.; Wang, Y. H. *J. Cryst. Growth* **2003**, *252*, 190.
(8) Tena-Zaera, R.; Katty, A.; Bastide, S.; Levy-Clement, C. *Chem. Mater.* **2007**, *19*, 1626.
(9) Platzer-Björkman, C.; Törndahl, I.; Hultqvist, A.; Kessler, J.; Edoff, M. *Thin Solid Films* **2007**, *515*, 6024.
(10) Zhang, B. P.; Wakatsuki, K.; Binh, N. T.; Usami, N.; Segawa, Y. *Thin Solid Films* **2004**, *449*, 12.
(11) Ohkubo, I.; Matsumoto, Y.; Ohtomo, A.; Ohnishi, T.; Tsukazaki, A.; Lippmaa, M.; Koinuma, H.; Kawasaki, M. *Appl. Surf. Sci.* **2000**, *159*, 514.
(12) Liu, W. R.; Hsieh, W. F.; Hsu, C. H.; Liang, K. S.; Chien, F. S. S. *J. Appl. Crystallogr.* **2007**, *40*, 924.
(13) Liu, W. R.; Li, Y. H.; Hsieh, W. F.; Hsu, C. H.; Lee, W. C.; Lee, Y. J.; Hong, M.; Kwo, J. *Cryst. Growth Des.* **2009**, *9*, 239.
(14) Lin, C. W.; Ke, D. J.; Chao, Y. C.; Chang, L.; Liang, M. H.; Ho, Y. T. *J. Cryst. Growth* **2007**, *298*, 472.
(15) Kowalik, I. A.; Guziewicz, E.; Kopalko, K.; Yatsunenko, S.; Wójcik-Głodowska, A.; Godlewski, M.; Dłużewski, P.; Łusakowska, E.; Paszkowicz, W. *J. Cryst. Growth* **2009**, *311*, 1096.
(16) Pung, S. Y.; Choy, K. L.; Hou, X.; Shan, C. *Nanotechnology* **2008**, *19*, 435609.
(17) Lin, P. Y.; Gong, J. R.; Li, P. C.; Lin, T. Y.; Lyu, D. Y.; Lin, D. Y.; Lin, H. J.; Li, T. C.; Chang, K. J.; Lin, W. J. *J. Cryst. Growth* **2008**, *310*, 3024.
(18) Lim, J.; Lee, C. *Thin Solid Films* **2007**, *515*, 3335.
(19) Wójcik, A.; Godlewski, M.; Guziewicz, E.; Minikayev, R.; Paszkowicz, W. *J. Cryst. Growth* **2008**, *310*, 284.
(20) Alessandri, I.; Zucca, M.; Ferroni, M.; Bontempi, E.; Depero, L. E. *Cryst. Growth Des.* **2009**, *9*, 1258.
(21) King, D. M.; Li, J.; Liang, X.; Johnson, S. I.; Channel, M. M.; Weimer, A. W. *Cryst. Growth Des.* **2009**, *9*, 2828.
(22) Puurunen, R. L. *J. Appl. Phys.* **2005**, *97*, 121301.
(23) Duniop, L.; Kursumovic, A.; MacManus-Driscoll, J. L. *Appl. Phys. Lett.* **2008**, *93*, 172111.
(24) Koyama, T.; Chichibu, S. F. *J. Appl. Phys.* **2004**, *95*, 7856.
(25) Wang, X. Q.; Iwaki, H.; Murakami, M.; Du, X. L.; Ishitani, Y.; Yoshikawa, A. *Jpn. J. Appl. Phys.* **2003**, *42*, L99.

(26) Chen, Y. F.; Bagnall, D. M.; Koh, H. J.; Park, K. T.; Hiraga, K.; Zhu, Z. Q.; Yao, T. *J. Appl. Phys.* **1998**, *84*, 3912.
(27) Ohkubo, I.; Ohtomo, A.; Ohnishi, T.; Mastumoto, Y.; Koinuma, H.; Kawasaki, M. *Surf. Sci.* **1999**, *443*, L1043.
(28) Vispute, R. D.; Talyansky, V.; Trajanovic, Z.; Choopun, S.; Downes, M.; Sharma, R. P.; Venkatesan, T.; Woods, M. C.; Lareau, R. T.; Jones, K. A.; Iliadis, A. A. *Appl. Phys. Lett.* **1997**, *70*, 2735.
(29) Vinnichenko, M.; Shevchenko, N.; Rogozin, A.; Grötzschel, R.; Mücklich, A.; Kolitsch, A.; Möller, W. *J. Appl. Phys.* **2007**, *102*, 113505.
(30) Abouzaid, A.; Ruterana, P.; Liu, C.; Morkoc, H. *Superlattices Microstruct.* **2007**, *42*, 110.
(31) D. Kohla, M. H.; G. Heilanda *Surf. Sci.* **1973**, *41*, 403.
(32) Hass, K. C.; Schneider, W. F.; Curioni, A.; Andreoni, W. *Science* **1998**, *282*, 882.
(33) Stampfl, C.; Van de Walle, C. G. *Phys. Rev. B* **1998**, *57*, R15052.
(34) Gerthsen, D.; Litvinov, D.; Gruber, T.; Kirchner, C.; Waag, A. *Appl. Phys. Lett.* **2002**, *81*, 3972.
(35) Vennegues, P.; Chauveau, J. M.; Korytov, M.; Deparis, C.; Zuniga-Perez, J.; Morhain, C. *J. Appl. Phys.* **2008**, *103*, 083525.
(36) Kawasaki, M.; Ohtomo, A.; Ohkubo, I.; Koinuma, H.; Tang, Z. K.; Yu, P.; Wong, G. K. L.; Zhang, B. P.; Segawa, Y. *Mater. Sci. Eng., B* **1998**, *56*, 239.